https://doi.org/10.5194/nhess-2022-256
Preprint. Discussion started: 24 October 2022


Natural Hazards and Earth System Sciences
Open Access
Discussions

# Instantaneous LEM back-analyses of major rockslides triggered during the 2016-2017 Central Italy seismic sequence

Luca Verrucci[1], Giovanni Forte[2], Melania De Falco[2], Paolo Tommasi[3], Giuseppe Lanzo[1], Kevin W. Franke[4], Antonio Santo[2]

[1] Dipartimento d'Ingegneria Strutturale e Geotecnica, Sapienza Università di Roma La Sapienza, Rome, Italy
[2] Dipartimento d'Ingegneria Civile, Edile e Ambientale; Università degli Studi di Napoli Federico II, Naples, Italy
[3] CNR – Istituto di Geologia Ambientale e Geoingegneria, Rome, Italy
[4] Department of Civil and Environmental Engineering, Brigham Young University, Provo, UT, USA

*Correspondence to*: Giovanni Forte (giovanni.forte@unina.it)

**Abstract.** Among the almost 1400 landslides triggered by the shocks of the 2016-2017 Central Italy seismic sequence, only a limited number, all classifiable as rockslides, involved volumes larger than 100 $m^3$. Four of these failures, including the three largest, were described in terms of structural and geomechanical investigations in a previous study. In this paper, the mechanics of these failures under seismic actions are investigated. The estimated acceleration time histories at the rockslide sites were evaluated through a 2D simplified numerical model accounting for the attenuation phenomena and for the topographic effect of the rock cliffs from which the slide detached. Instantaneous stability analyses were carried out to obtain insights into the variability of the instantaneous margin of safety along the development of the shocks over the entire spectrum of mechanisms that could be activated. Finally, some general suggestions on the pseudo-static verification method for three-dimensional cases are proposed, which represent useful indications to hazard evaluation at local and regional scale.

## 1 Introduction

Most of the landslides occurred in Central Italy during the earthquakes of the last century are rock falls or rockslides (**Martino *et al.* 2017; Esposito *et al.* 2000**). The latter have involved relatively small rock volumes in comparison to most of the rockslides reported in literature (**Lombardo *et al.* 2021**, **Quinton Aguilera *et al.* 2022**), for the energy released by these seismic events (moment magnitude, $M_w \leq 6.5$). Similarly to many other earthquake-triggered landslides (**Rodriguez *et al.* 1999**), they were characterized by a marked disruption of the rock mass and originated on steep slopes, where inertial forces easily remove well-delimited and scarcely constrained blocks from the slope through rigid sliding/toppling or tensile failures of overhanging blocks. All these instability phenomena are very "brittle", i.e., relatively small displacements develop before the constraints change abruptly and a fast propagation phase begins with a free fall of single or multiple non-interacting blocks.

https://doi.org/10.5194/nhess-2022-256
Preprint. Discussion started: 24 October 2022



Since seismic loading acts only at the early detachment of earthquake-triggered rock failures (propagation is controlled only by gravity loading and slope geometry) the study of this stage is very important for local hazard evaluation. Literature has evidenced that the intrinsic key factors influencing the seismic activation of these landslides include the structural features of the rock mass (e.g. joint spacing and orientation, presence of major joints), the topographic modifications to ground motion, and the hydraulic conditions (e.g., **Massey *et al.*, 2017; Pignalosa *et al.*, 2022; Sepúlveda *et al.*, 2005a,b; Tsou *et al.*, 2018**). These considerations sparkled investigation of the failure stages of the largest rockslides occurred during the 2016-2017 Central Italy seismic sequence (CISS), which lasted from August 2016 to mid-January 2017 and counted several shocks ranging from $M_w$ 5 to $M_w$ 6.5 (the latter the highest magnitude recorded in Central Italy during the last century, **Rovida *et al.*, 2019**). The mobilized volumes ranged from a few m$^3$ to several thousands of m$^3$; all the largest rockslides were triggered by shocks with $M_w$ >5. The general features of the largest rockslides were described by **Forte *et al.* (2021)**, **Lanzo *et al.* (2019)**, **Franke *et al.* (2019) and Romeo *et al.* (2017)**. Four of them are analysed in this paper.

Analyses were conducted with the instantaneous limit equilibrium method (LEM) by applying the acceleration histories of the main earthquake shocks. Input data were collected during several investigation campaigns that included aero-photogrammetric surveys with unmanned aerial vehicles (UAVs), sampling of blocks and joints and direct *in-situ* measurements of joint orientation, spacing and roughness. Data and results of the reconnaissance investigations are reported in detail by **Forte *et al.* (2021)**, who identified the surfaces delimiting the detached rock wedges and referred them to the general tectonic setting of the area.

For each rockslide, after a kinematic analysis in static conditions (Sect. 2), the seismic motion responsible of failure was estimated in two steps (Sect. 3): a ground motion prediction equation was applied first to the available ground motion records to account for attenuation at the rockslide sites, then modifications to ground motion induced by the slope morphology were evaluated through a general simplified 2D numerical model that reproduces the main resonance and attenuation phenomena affecting very steep rock slopes during seismic shocks. Finally, the behaviour of the rock wedges during the shocks was analysed using the instantaneous limit equilibrium procedure (Sect. 4) in the instrumental hypothesis that they moved rigidly with the surrounding rock mass. The volumes of the rockslides are in fact small enough to represent the primary mechanism of failure as a rigid wedge (**Hungr *et al.* 2014**) and to explore the role of the inertial forces in inducing failure. At this early stage, very small displacements occurred mainly as sliding, and the constraint configuration was dictated by the original orientation of pre-existing joints. The possible subsequent kinematic evolution (e.g. toppling), the disarrangement of the wedge and the start of the propagation phase are out of the scope of this note.

## 2 Examined rock-slides

Local geology, rock mass structure, major joints delimiting the failed mass and wedge volumes of the selected four Central Italy rockslides examined in this study are described in detail by **Forte *et al.* (2021)**. Features of these events and their possible triggering earthquakes are shown in **Table 1**, while their location is reported in **Figure 1** together with the epicentres of the main shocks of the CISS.

https://doi.org/10.5194/nhess-2022-256
Preprint. Discussion started: 24 October 2022


Natural Hazards and Earth System Sciences Open Access
Discussions

Figures 2a through 2d present post-collapse frontal views of the rockslides. All the failure scars are carved in sound limestone, either layered or relatively massive. The wedges were delimited by near-planar surfaces (labelled in Figure 2), which are single major joints, excepting for the Rubbiano rockslide, which was delimited at its back by a combination of several discontinuities of fairly limited extent. Figure 2 also includes stereo-plots with great circles of the planes delimiting each wedge at the very beginning of the detachment, as estimated from the 3D models and point clouds obtained from UAV aerial surveys (**Franke *et al.* 2019; Tommasi *et al.* 2019**). Great circles refer to single major joints or to planes interpolating combinations of minor joints.

## 3 Seismic input at the rockslide sites

The shaking level at each rockslide site was assessed in two steps: 1) estimation of the ground shaking on a horizontal rigid outcrop, beginning with the available recordings of the shocks, attenuated with an appropriate Ground Motion Prediction Equation (GMPE); and 2) calculation of the ground motion modification due to the local rock slope morphology. Ground modification induced by stratigraphic conditions were not considered because for all slides the bedrock and possible differences of rock mass quality within the same slope were considered negligible.

The scrutiny of Google Earth satellite images taken at different dates over 2016, indicates that Nera and Rubbiano rockslides occurred during the strongest shock of the seismic sequence (Norcia, October 30th, $M_w$= 6.5). Piè la Rocca slide occurred during one of the two August 24th shocks: the $M_w$= 6.0 Accumoli shock or the $M_w$= 5.3 Norcia shock, the latter having an epicentre very close to the site (4.2 km). Costa Cattiva rockslide occurred during one of the two October 26th shocks: either the $M_w$= 5.4 Visso shock or the $M_w$= 5.9 Castelsantangelo shock. Table 2 summarizes the main features of these shocks obtained from signals recorded at the neighbouring accelerometric stations on stiff ground (Engineering Strong-Motion Database, ESM, **Luzi *et al.* 2016**).

The estimate of peak ground acceleration, PGA, calibrated with an appropriate GMPE at each of the four rockslide sites is presented in Figure 3. Diamonds represent the measured PGAs of the horizontal components (i.e., geometric mean of East and North components) versus the Joyner–Boore distance ($D_{JB}$) of the station. These measurements were interpolated with and calibrated against the GMPE of **Bindi *et al.* (2011)** (solid lines in Figure 3). The site class A (rigid ground, according to Eurocode 8, **EN 1998-5:2004**). and the normal fault class were used in the GMPE, while the moment magnitude was used as the regression parameter. The PGA at the sites were finally estimated using the $D_{JB}$ of each site on the interpolated GMPE (full blue circle symbols in Figure 3). The complete accelerograms were obtained by scaling all the components recorded at the closest station on rock outcrop to the PGA with the same scaling factors, *S*. The parameters used in both the GMPE calibration and scaling procedure are shown in Table 3.

Since the failed rock slopes are not accessible for geophysical investigation, the shear wave velocity to be used in seismic response assessment was estimated based on results of borehole geophysics conducted on the same geological formations at neighbouring sites having similar fracturing and loosening of the rock mass. Down holes in the *Maiolica formation* conducted in the framework of the third level seismic microzonation of the struck area (*Banca dati*

https://doi.org/10.5194/nhess-2022-256
Preprint. Discussion started: 24 October 2022



*microzonazione sismica*, www.webms.it) indicated that pervasively fractured rock (i.e. with RQD values close to 0) exhibits a $V_s$ of about 600 m/s, which increases to 2000 m/s in a fairly jointed rock mass.

The investigated slopes can be roughly assimilated to steep flanks of deep valleys (200-500 m) separated by large and relatively flat mountain ridges. The modifications to the ground motion that the general slope morphology produces at each site were estimated through a finite difference model that simulates the visco-elastic dynamic behaviour of a simplified slope: a step-like slope with a vertical cliff of height $H$ and upstream and downstream horizontal areas (**Figure 4a**). The effects of step-like slope topography on seismic motion have been studied by many authors: **Ashford *et al.* (1997)**, **Bouckovalas & Papadimitriou (2005)**, **Nguyen & Gatmiri (2007)**, **Lenti & Martino (2012)**, **Li *et al.* (2019)**. It is valuable to investigate the general influence of very steep slopes, like those from which the rockslides detached, because the vertical cliff is an extreme schematization that is not investigated in details by the literature.

In the frequency domain, the modification of a harmonic motion of wavelength $\lambda$ (frequency $f$) propagating in a medium with shear wave velocity $V_S$ and Poisson ratio $\nu$, can be expressed by the amplification ratio $A$ between the amplitude at a point at height $h$ on the slope face and the amplitude on the horizontal rigid outcrop. In a dimensional analysis approach, $A$ can be expressed as a function of the dimensionless variables $\zeta$, $\eta$, $\nu$, being $\zeta = h/H$ and $\eta = H/\lambda = Hf/V_S$.

If planar vertically propagating waves are considered, two cases (P- and S-waves) are sufficient to estimate the variability of $A$ along the entire vertical wall ($\zeta$ in the range 0.0-1.0). To cover a sufficiently broad frequency range ($\eta$=0.03-2.0), two analyses were performed for each wave type using Ricker waves with different frequency content as input motion.

The model was built in the 2D finite difference code FLAC (**Itasca 2011**). A slope height of 100 m and elastic properties $V_S$ = 100 m/s and $\nu$ = 0.3 was considered, but the normalized results can be extended to a cliff of different height and stiffness thanks to the principle of linear superposition. The model bottom is an absorbing viscous boundary, whilst free-field boundary conditions are applied to the lateral boundaries, which are located at least five times $H$ from the slope face. A Rayleigh formulation was assumed with a uniform critical damping ratio of $D$ = 0.5%.

The results are presented in the plots of amplification ratios of the normal ($A_n^P$, $A_n^S$) and vertical ($A_z^P$, $A_z^S$) component, for the incoming P- and S-waves (**Figure 4b**), and are functions of $\zeta$ and $\eta$. Along a horizontal line (i.e., at constant $\zeta_0$), the diagrams give the amplitude of the transfer functions from the outcrop motion (horizontal and vertical component, respectively, for the incoming S- and P-waves) to the motion of a point at height $h=\zeta_0 H$ on the cliff.

According to literature results (**Ashford *et al.* 1997; Assimaki *et al.* 2005**), for the incident S waves the most amplified wavelength corresponds to the first normalized modal frequency of 0.2, with a peak of $A_n^S$ greater than 1.4. For the Nera rockslide ($H$= 400m), the main resonance frequency, which is about 1.0 Hz, is critical along almost the entire cliff, although amplification decreases as elevation decreases. In addition, at medium and lower elevations, the higher frequencies are reduced overall. The vertical component produced by incident S-waves has significant amplitude ratios $A_z^S$ only at the crest and for normalized frequencies in the wide range 0.4-1.4 (e.g., 2.0 – 7.0 Hz for the Nera case with about $V_S$ = 2 km/s).

https://doi.org/10.5194/nhess-2022-256
Preprint. Discussion started: 24 October 2022



The amplification ratios for incident P waves, $A_n^P$ and $A_z^P$ reveal a main amplification of the vertical component at the crest and at almost the whole vertical wall for a normalized frequency of about 0.1 (0.5 Hz for the Nera case). Conversely, the horizontal component is flattened all along the cliff wall for all frequencies ($A_n^P < 0.8$).

The linear process used to assess the motion at the elevation of the centre of gravity of the rockslide proceed as follows. Since the normal (horizontal) and vertical components $a_n$ and $a_z$ of the outcrop acceleration can be considered equivalent, respectively, to an S- and a P-wave in a vertical plane normal to the slope face, their Fourier transform $a_n(\eta)$ and $a_z(\eta)$ are multiplied to the transfer (amplification) functions to obtain the output components on the cliff (i.e., after morphological modifications). These are successively combined:

$$a_{out,n}(\eta) = A_n^S(\eta,\zeta_0)a_n(\eta)+A_n^P(\eta,\zeta_0)a_z(\eta) \quad (1a)$$

$$a_{out,z}(\eta) = A_z^S(\eta,\zeta_0)a_n(\eta)+A_z^P(\eta,\zeta_0)a_z(\eta), \quad (1b)$$

where $\zeta_0=h_0 / H$ is the normalized height of the rockslide gravity centre. Finally the acceleration vector $\vec{A}(\zeta_0,t)$ is obtained by applying the inverse Fourier transform to the (1) and assuming a shear wave velocity of 2200 m/s at all sites. The infinite stiffness of the model slope along the slope strike entails that the component $a_p(t)$ is unmodified. The geometrical and morphological features that control the response calculations are shown in **Table 4** for each rockslide.

In **Figure 5** the amplification/attenuation effects are described through comparing the acceleration response spectra (damping 5%) of the two motions for all the considered shocks and for both the horizontal (normal) and vertical components. The alteration of the motion is usually significant for periods lower than 1-2 s, while it is negligible for periods higher than the fundamental period $T_0$ of the first vibration mode of the cliff ($\lambda = 5H$) indicated by vertical dotted lines.

These analyses aim to estimate the general modifications to the seismic motion caused by large scale morphological features. Nonetheless, local irregularity of the slope surface like sharp ridges, spurs and pinnacles, which can induce significant further local amplifications/attenuations especially for small volumes, are not considered in the present research.

## 4 Seismic back analysis

**Forte *et al*. (2021)** presented a first set of static LEM back analyses with the landslide body subjected to gravity load only; geometry and strength parameters adopted in the analyses are shown in **Table 5**. Under the same assumptions of these static analyses (absence of water pressure and planar sliding surfaces with a Mohr-Coulomb strength criterion), the time histories of the safety factors during the shocks were evaluated for the rockslides. Only translational sliding mechanisms were considered, because their predominant role in driving the wedges to the collapse clearly emerged (**Forte *et al*., 2021**).

The strength parameters used by **Forte *et al*. (2021)** were derived from direct in situ investigations at the rockslide sites and on laboratory tests on samples collected both at the rockslide sites and at neighbouring sites in the same geological formations involved in the rockslides. The friction angle along the sliding planes varies between 40° and 47° depending on the local roughness and waviness. Intact rock bridges along the joints forming the slide scar, which broke during sliding, were observed on close UAV images. Their contribution to joint cohesion was evaluated as the cohesive component of the shear strength of the rock mass ($c_{rb}$ = 570 kPa) multiplied by the area $A_{rb}$ of the rock bridges. The parameter $c_{rb}$ was

https://doi.org/10.5194/nhess-2022-256
Preprint. Discussion started: 24 October 2022



estimated by linearizing the Hoek Brown strength envelope of the rock mass, obtained from the strength envelope of the rock material scaled through the Geological Strength Index, *GSI*, determined on the rock outcrops at the rockslide sites (**Hoek *et al.* 2002**).

High resolution imagery captured from UAVs and during helicopter surveys over the Nera slide revealed that the tip of the sliding surface appeared to be irregular and paler than the surrounding rock mass. This evidence induced **Forte *et al.* (2021)** to hypothesize that the lower part of the failure surface developed through the rock mass rather than along an existing joint. Therefore, an additional contribution was considered by multiplying the cohesion $c_{rb}$ by the area (800 m$^2$) of the failure surface at the wedge tip.

For the Rubbiano rockslide (RB), a tensile strength equal to 10% of the rock mass cohesion $c_{rb}$, was considered as an additional strength contribution that contrasted the detachment from plane 1 (**Figure 2d**). Where the plane 3 is present (as at the top of Piè la Rocca rockslide, **Figure 2c**) the wedge detaches along it from the rock mass behind, thus providing no strength contribution.

Variable inertial forces $\vec{I}(t) = -m\vec{A}(t)$ were added to equilibrium equations, applied uniformly to the rigid blocks with mass $m$. This procedure is mechanically consistent only as long as the block does not displace with respect to the rock mass and therefore it only provides a realistic assessment immediately before sliding begins. In fact the relative motion alters the inertial forces with respect to those calculated with the base acceleration and furthermore reduces the strength due to progressive smoothing of the joint surface and failure of the rock bridges. For these reasons the safety factor ($F_S$) during seismic excitation calculated through this analysis is intended to identify the most probable instants of failure initiation and the critical mechanisms. This type of calculation also represents an instrument to weight the relative importance of sliding mechanisms during shaking and thus to better handle the pseudo-static analysis method. Safety factors is calculated for the whole shaking duration and in turn it could assume also values lower than 1.0 during some time intervals.

In resolving equilibrium and calculating $F_S$, the activation of a different translational mechanism with respect to that occurring in static conditions was also considered. In fact the instantaneous sliding mechanism is controlled by the current direction of the resultant external force, which in a dry slope coincides with the sum of the block weight and the inertial force. The kinematical regions of the space in the stereographic projection corresponding to different mechanisms **(Londe *et al.* 1969)** are reported in **Figure 6**, the static resultant (weight) direction being indicated through red circles. The number of passages between different mechanisms during the seismic event is related to the oscillation amplitude of the resultant force and to the distance of its pole from the kinematical region boundaries.

The instantaneous $F_S$ for the Mohr-Coulomb strength criterion can be calculated trough Eq. (2) and (3) in case of sliding along a single plane or both planes, respectively:

$$F_S = \frac{cA+N\,tg\varphi}{T} \tag{2}$$

$$F_S = \frac{c_1A_1+N_1tg\varphi_1+c_2A_2+N_2tg\varphi_2}{T_{12}} \tag{3}$$

https://doi.org/10.5194/nhess-2022-256
Preprint. Discussion started: 24 October 2022




*N* and *T* in Eq. (2) are the normal and tangential components of the resultant acting on a single sliding plane. $T_{12}$, $N_1$ and $N_2$ in Eq. (3) are the components of the resultant force parallel to the intersection line $I_{12}$ of planes 1 and 2 and normal to the planes, respectively. *c*, *φ* and *A* are the cohesion, friction angle and the contact areas, respectively; subscripts refer to the plane. The passage from one mechanism to another one entails an instantaneous change in the $F_S$ value.

For each analysis, the activated mechanisms and the time histories of $F_S$ are reported in **Figure 7**. For instance, the mechanism of the Nera rockslide (**Figure 7a**) changes from sliding along the $i_{12}$ to sliding along the single plane 2. The latter mechanism has a quite lower level of safety and the $F_S$ repeatedly crosses the critical threshold $F_S = 1$ during the shock. This means that the available strength was reached since the very first oscillations and irreversible displacements grew up towards collapse. In cases similar to the Nera slide, a high $F_S$ evaluated in static conditions is not meaningful in evaluating the “distance” from failure in seismic conditions: also for moderate shaking a very small deviation of the resultant force from the vertical direction can be sufficient to activate a less safe sliding mechanism.

Due to the geo-structural setting and the amplitude of the examined seismic shocks, the analysis of the Costa Cattiva rockslide yields a sliding mechanism along the line $i_{12}$ both in static and dynamic condition (**Figure 7b**). The position of the blocks produced by the rock avalanche that followed the wedge failure confirms this mechanism. For both the October 26$^{th}$ shocks, the analyses do not justify the Costa Cattiva failure in seismic conditions (i.e., the computed $F_S$ is > 1). Since an overestimation of the strength is improbable due to the simple structural conditions and the low joint roughness, this result is likely explained by having neglected the small-scale amplification. The wedge was in fact located on top of a narrow sharp ridge protruding from the slope.

The analysis of Piè la Rocca slide (**Figure 7c**) helped also to assess that the wedge likely failed during the Norcia event ($M_W$=5.3). In fact, in the earlier event (Accumoli, $M_W$=6.0), $F_S$ trespasses the stability threshold only once and for a very short time span, which could cause only very small displacements without reaching full collapse. Although the displacements experienced by the rockslide and the maximum available displacement before the collapse were not estimated, the geometric layout of the rockslide scar suggests that the wedge should have experienced displacements as large as to break a constraining rock spur at its highest part. At Piè la Rocca rockslide, the frequent switches between the two sliding modes determine a change in $F_S$ that is not as important as for the Nera slide because the two mechanisms have quite similar safety margins against failure.

The Rubbiano rockslide (**Figure 7d**) maintains a unique mechanism during the application of the acceleration history, and despite the significant epicentral distance (7 km), the available strength was exceeded several times during the strong $M_w$-6.5 shock. The structural layout of the slide scar and the slenderness of the detached wedge (small thickness normal to the cliff in comparison to the large extent parallel to the cliff) indicate that very small displacements were sufficient to reach the collapse, likely favoured by a rocking effect.

Along the time histories shown in **Figure 7**, the values of $F_S$ are highlighted for particular instants: when the components along the geographical directions (E-W, N-S, Up-Down) and the horizontal component of the acceleration reach their maximum absolute values (respectively *x, y, z, h* points in **Figure 7**), and when the acceleration vector magnitude

Natural Hazards and Earth System Sciences
Open Access
EGU
Discussions

reaches its maximum value (*m* points in **Figure 7**). It is apparent that, despite at these instants the inertial force is quite high, $F_S$ is not always near its minimum. For some cases (e.g. *x, h, m* conditions of Costa Cattiva slide and Piè la Rocca slide during the Oct. 26$^{th}$ shock) these instants even correspond to the maximum values of $F_S$.

Different instantaneous $F_S$ values are also highlighted when the maximum values of particular acceleration components (all slopewards and related to the geometry and orientation of the slope) are reached. These are the dip direction of the rock face (*n* points in **Figure 7**), the intersection line between the two main sliding planes (*i12* points in **Figure 7**), and the dip directions of the two planes (*p1* and *p2* points in **Figure 7**;). The results show that both *n* and *i12* conditions give the minimum $F_S$ or a value near to the minimum of the entire shock. The only exception is represented by the *i12* condition for the Nera slide. In this case, the resultant force falls in the region of the safer between the two possible mechanisms and *i12* condition gives $F_S = 1.5$, i.e., much higher than the minimum value ($F_S = 0.83$).

These observations provide some clues for a rational choice of the direction of the inertial force to be applied on a 3D rock wedge in pseudo-static stability analyses. Due to the significant anisotropy of the mechanical problem, the inertia calculated at instants when the magnitude of the acceleration vector or that of some pre-defined components are maximum can have negligible or favourable influence on stability. Conversely, the resistance to sliding can be overcome when the component along more adverse directions, either that along *p1*/*p2* or *i12*, is significant. The orientation of the resultant forces determining the minimum $F_s$ (stars in **Figure 6**) always falls within sectors delimited by these two directions (thick dashed lines in **Figure 6**). Application of the pseudo-static inertial force along these two directions yields the most conservative result only on condition that they involve all the possible sliding mechanisms. Otherwise, if both these directions correspond to the same mechanism, other orientations of the inertial force should also be tested to verify the activation of different mechanisms.

## 5 Discussion and conclusions

Stability analyses in static and seismic conditions were performed on four rockslides occurred during the main shocks of the 2016-2017 Central Italy seismic sequence. The failed masses can be realistically schematized with wedges delimited by two intersecting planar discontinuities and possibly by a detachment surface at their back. The activated primary mechanisms were sliding along either one plane or the intersection line between two planes. These mechanisms developed until the wedges lost their constraints and rock falls/avalanches started. The volume of the rockslides (not exceeding 32,000 m$^3$) is small enough to assume an initial rigid motion of the wedges.

The available ground motion measurements were interpolated with an attenuation law with fixed source mechanism and stiffness class. Then a simple visco-elastic model was implemented in a parametric finite difference stress-strain analysis to calculate motion modifications due to the morphologic conditions, i.e. a step-like rock slope. Both the normalized results and the applications to the actual rockslide sites show that significant horizontal amplification is expected almost only at the crest while at intermediate heights the main effect is a reduction of the horizontal component and an amplification of the vertical one. Cyclic strength degradation is another important issue that seems to have played an important role in most of

https://doi.org/10.5194/nhess-2022-256
Preprint. Discussion started: 24 October 2022



the major rockslides described in the previous sections. The high number of loading cycles applied during the main earthquakes seem to have especially affected the rock bridges along persistent joints of the limestone formations, both under shear and in tension. In this respect, static limit equilibrium back analyses of the Nera rockslide indicate that rock bridges were necessary to ensure stability even in static conditions and also provided sufficient strength to maintain the wedge stable during the October 26th $M_w$6.0 event. Shear strength was most likely overcome during the successive October 30th $M_w$6.5 shock.

The examined rockslides, which represent four of the largest landslides that occurred during the 2016-2017 sequence, are all characterized by a highly asymmetric wedge shape. This entails a low factor of safety due to the reduced (even null) strength contribution along one of the wedge planes. Even the static LEM stability analyses showed that the potential mechanisms are often not univocally established. In fact, either minor modifications of the geometrical layout or a small deviation of the resultant of external forces can activate a different mechanism with respect to that initially hypothesized. A clear representation of this problem can be obtained in the stereographic projection by subdividing the direction space into regions associated to different mechanisms. The variability of the mechanism is particularly significant in seismic conditions when the inertial force is addedd to the weight of the blocks thus making the resultant force fluctuating around its initial orientation.

The instantaneous LEM back analyses, carried out under the hypothesis that blocks are rigidly connected to the underlying bedrock, showed that also the safety margin can deeply fluctuate during the shock as a function of the mechanisms that are potentially activated. The minimum safety factor during the shock does not necessarily coincide with the typical directions of the pseudo-static force in a classic pseudo-static analysis (normal to the slope face or along the line of intersection between the sliding planes). Therefore, direction is to be varied through a rational and complete examination of all the possible mechanisms.

These results also indicate that specific structural features of the slope must carefully be accounted for in evaluating potential hazard on rock slopes overlooking infrastructures and inhabited areas. This issue affects risk analysis not only at local scale but also for long stretches of valley flanks overlooking transportation infrastructures in mountainous regions. In this respect, a fundamental resource is gained through the application of UAV surveys, which give the possibility of extending quantitative investigations to long infrastructure stretches at affordable times and costs, and to slopes inaccessible even to remote terrestrial surveys. Quantitative investigations involve not only determination of geometry and structural setting of the slope, but also geomechanical parameters as medium- to large-scale roughness and extent of the rock bridges along major joints.

- **Code availability** NOT APPLICABLE
- **Data availability** NOT APPLICABLE

• **Author contribution** L.V. conceptualization, formal analysis and software, writing-original, writing-review, visualization; G.F. and M.D.F.: geological investigation, writing-original, writing-review, visualization, PT: conceptualization, geotechnical investigation, funding acquisition, writing-review; GL: supervision, writing-review, funding acquisition, KF: UAV investigation, writing-review, funding; AS: investigation, supervision, funding acquisition

**Competing interests** The authors declare that they have no conflict of interest.

**Funding:**

The research was partially funded by the Italian Civil Protection Department RELUIS project (2018), PR8-UR18-WP2 UNINA (P.I. A. Santo), Progetto di Ateneo Sapienza 2017 "Site investigations, monitoring and modelling of earthquake induced rockslides triggered by the 2016-2017 Central Italy seismic sequence" (P.I. G. Lanzo), P. Tommasi was funded by Progetto Fra.Si. funded by Italian Ministry for Ecological Transition (P.I. P. Reichenbach). K. Franke was funded by a Mentored Research Grant (MRG) from the Brigham Young University Ira A. Fulton College of Engineering and the Center for Unmanned Aircraft Systems (C-UAS), the National Science Foundation Industry/University Cooperative Research Center (I/UCRC) under NSF Award No. IIP-1650547, along with significant contributions from C-UAS industry members.

**Acknowledgements**

Eng. Valentina Tuccio carried out preliminary seismic response analyses for the Nera River Valley rockslide. The Authority for the Sibillini Mts. National Park (Dr. A. Rossetti) and Dipartimento della Protezione Civile (Engg. P. Pagliara and P. Bertuccioli) are acknowledged for allowing surveys in the park area and for access to landslide areas during the Seismic emergency, respectively. BYU undergraduate students Bryce Berrett, Nicole Hastings, Jeffery Derricott, Bridgette Ostrum, Doug Graff, and graduate student Michael Freeman contributed significantly to the UAV fieldwork and development of the 3D reconstructions of the rock falls.

**References**

Aguilera, Q., Lombardo, L., Tanyas, H. and Lipani, A.: On the prediction of landslide occurrences and sizes via Hierarchical Neural Networks. Stochastic Environmental Research and Risk Assessment, 36, 2031–2048. https://doi.org/10.1007/s00477-022-02215-0, 2022.

Ashford, S.A., Sitar, N., Lysmer, J., and Deng, N.: Topographic effects on the seismic response of steep slopes. Bull Seismol Soc Am 87(3): 701–709, https://doi.org/10.1785/BSSA0870030701 , 1997.

Assimaki, D., Kausel, E., and Gazetas, G.: Wave propagation and soil–structure interaction on a cliff crest during the 1999 Athens Earthquake. Soil Dyn Earthq Eng 25: 513–527 doi:10.1016/j.soildyn.2004.11.031, 2005.

https://doi.org/10.5194/nhess-2022-256
Preprint. Discussion started: 24 October 2022




Bindi, D., Pacor, F., Luzi, L., Puglia, R., Massa, M., Ameri, G., Paolucci, R.: Ground motion prediction equations derived from the Italian strong motion database. Bull Earthquake Eng 9:1899–1920 doi:10.1007/s10518-011-9313-z, 2011.

Bouckovalas, G.D., Papadimitriou, A.G.: Numerical evaluation of slope topography effects on seismic ground motion. Soil Dyn Earthq Eng 25, 547-558 doi:10.1016/j.soildyn.2004.11.008, 2005.

Esposito, E., Porfido, S., Simonelli, A.L., Mastrolorenzo, G., and Iaccarino G.: Landslides and other surface effects induced by the 1997 Umbria–Marche seismic sequence. Eng Geol 58 353–376, doi: 10.1016/S0013-7952(00)00035-1, 2000.

EN 1998-5:2004 Eurocode 8: Design of structures for earthquake resistance – Part 5: Foundations, retaining structures and geotechnical aspects https://eurocodes.jrc.ec.europa.eu/.

Forte, G., Chioccarelli, E., De Falco, M., Cito, P., Santo, A., and Iervolino, I.: Seismic soil classification of Italy based on surface geology and shear-wave velocity measurements. Soil Dyn. Earthq. Eng., 122: 79-93, https://doi.org/10.1016/j.soildyn.2019.04.002, 2019.

Forte, G., Verrucci, L., Di Giulio, A., De Falco, M., Tommasi, P., Lanzo G., Franke K.W. and Santo A.: Analysis of major rock slides that occurred during the 2016–2017 Central Italy seismic sequence. Eng Geol 290, 106194 https://doi.org/10.1016/j.enggeo.2021.106194, 2021.

Franke, K.W., Lingwall, B.N., Zimmaro, P., Kayen, R.E, Tommasi, P., Chiabrando, F. and Santo, A.: Phased reconnaissance approach to documenting landslides following the 2016 Central Italy Earthquakes. Earthquake Spectra 34, 4, 1693-1719 https://doi.org/10.1193/082117EQS165M, 2019.

Hoek, E., Carranza-Torres, C., and Corkum, B.: Hoek-Brown failure criterion – 2002 Edition. 5th North American Rock Mech. Symp. & 17th Tunneling Association of Canada Conf., NARMS-TAC, Toronto, 267-271, 2002.

Hungr, O., Leroueil, S., Picarelli, L.: The Varnes classification of landslide types, an update. Landslides 11, 167–194 https://doi.org/10.1007/s10346-013-0436-y, 2014.

Itasca: FLAC-Fast Lagrangian Analysis of Continua, Ver. 7.0. User's Guide. Itasca Cons Group, Minneapolis, USA, 2011

Lanzo, G., Tommasi, P., Ausilio, E., Aversa, S., Bozzoni, F., Cairo, R., d'Onofrio, A., Durante, M.G., Foti, S., Giallini, S., Mucciacciaro, M., Pagliaroli, A., Sica, S., Silvestri, F., Vessia, G., and Zimmaro, P.: Reconnaissance of geotechnical aspects of the 2016 Central Italy earthquakes. Bull Earthquake Eng 17, 5495–5532 doi: 10.1007/s10518-018-0350-8, 2019.

Lenti, L, and Martino, S.: The interaction of seismic waves with steplike slopes and its influence on landslide movements. Eng Geol 126:19–36, doi:10.1016/j.enggeo.2011.12.002, 2012.

Li, H., Liu, Y., Liu, L., and Xia, X.: Numerical evaluation of topographic effects on seismic response of single-faced rock slopes. Bull Eng Geol Environ 78, 1873–189,1 https://doi.org/10.1007/s10064-017-1200-7, 2019.

Lombardo, L., Tanyas, H., Huser, R., Guzzetti, F. and Castro-Camilo, D.: Landslide size matters: A new data-driven, spatial prototype. Engineering Geology, 293, 106288, https://doi.org/10.1016/j.enggeo.2021.106288., 2021.

https://doi.org/10.5194/nhess-2022-256
Preprint. Discussion started: 24 October 2022

Natural Hazards and Earth System Sciences
Discussions

Londe, P., Vigier, G., and Vormeringer, R.: Stability of rock slopes, a three-dimensional study. J Soil Mech and Found Div ASCE, 95 (SM1), 235-262, 1969.

Luzi, L., Puglia, R., Russo, E., and ORFEUS WG5: Engineering Strong Motion Database, ver 1.0. Istituto Nazionale di Geofisica e Vulcanologia, Observatories & Research Facilities for European Seismology, doi:10.13127/ESM, 2019.

Martino, S., Bozzano, F., Caporossi, P., D'Angiò, D., Della Seta, M., Esposito, C., Fantini, A., Fiorucci, M., Giannini, L.M., Iannucci, R., Marmoni, G.M, Mazzanti, P., Missori, C., Moretto, S., Rivellino, S., Romeo, R.W, Sarandrea, P., Schilirò, L., Troiani, F., and Varone, C.: Ground Effects triggered by the 24th August 2016, Mw 6.0 Amatrice (Italy) earthquake: Surveys and inventorying to update the CEDIT catalogue. Geografia Fisica e Dinamica Quaternaria, 40, 1, 77-95, doi:10.4461/GFDQ.2017.40.7, 2017.

Massey, C., Della Pasqua, F., Holden, C., Kaiser, A., Richards, L., Wartman J., McSaveney, M.J., Archibald, G., Yetton, M., and Janku, L.: Rock slope response to strong earthquake shaking. Landslides 14, doi: 10.1007/s10346-016-0684-8, 249–268, 2017.

Nguyen, K.V., and Gatmiri, B.: Evaluation of seismic ground motion induced by topographic irregularities. Soil Dyn Earthq Eng 27, 183–188 doi: 10.1016/j.soildyn.2006.06.005, 2007.Rodriguez C., Bommer J., and Chandler R.: Earthquake-induced landslides: 1980–1997. Soil Dyn Earthq Eng, 18, 325-346., doi:10.1016/S0267-7261(99)00012-3, 1999.

Pignalosa, A., Forte, G., Budetta, P., and Santo, A.: Topographic amplification and debris remobilization as a cause for increasing rockfall hazard in seismic areas: A case study in Central Italy. Geomorphology, 403, 108160, doi: 10.1016/j.geomorph.2022.108160, 2022.

Romeo, S., Di Matteo, L., Melelli, L., Cencetti, C., Dragoni, W., and Fredduzzi, A.: Seismic-induced rockfalls and landslide dam following the October 30, 2016 earthquake Central Italy. Landslides 14, 1457–1465, doi:10.1007/s10346-017-0841-8, 2017.

Rovida, A., Locati, M., Camassi, R., Lolli, B., and Gasperini, P.: Catalogo Parametrico dei Terremoti Italiani (CPTI15), versione 2.0. Istituto Nazionale di Geofisica e Vulcanologia (INGV). https://doi.org/10.13127/CPTI/CPTI15.2, 2019.

Sepúlveda, S.A., Murphy, W., Jibson, R.W., and Petley, D.N.: Seismically induced rock slope failures resulting from topographic amplification of strong ground motions: The case of Pacoima Canyon, California. Eng Geol 80 336– 348, https://doi.org/10.1016/j.enggeo.2005.07.004, 2005a.

Sepúlveda, S.A., Murphy, W., and Petley, D.N.: Topographic controls on coseismic rock slides during the 1999 Chi-Chi earthquake, Taiwan. Quart J Eng Geol Hydrog, 38, 189–196, https://doi.org/10.1144/1470-9236/04-062, 2005b.

Stewart, J.P., Zimmaro, P., Lanzo, G., Mazzoni, S., Ausilio, E., Aversa, S., Bozzoni, F., Cairo, R., Capatti, M.C., Castiglia, M., Chiabrando, F., Chiaradonna, A., d'Onofrio, A., Dashti, S., De Risi, R., De Silva, F., Della Pasqua, F., Dezi, F., Di Domenica, A., Di Sarno, L., Durante, M.G., Falcucci, M., Foti, S., Franke, K.W., Galadini, F., Giallini, S., Gori, S., Kayen, R.E., Kishida, T., Lingua, A., Lingwall, B.N., Mucciacciaro, M., Pagliaroli, A., Passeri, F., Pelekis, P., Pizzi, A.,

https://doi.org/10.5194/nhess-2022-256
Preprint. Discussion started: 24 October 2022


Reimschiissel, B., Santo, A., Santucci De Magistris, F., Scasserra, G., Sextos, A., Sica, S., Silvestri, F., Simonelli, A.L., Spano, A., Tommasi, P., and Tropeano, G.: Reconnaissance of 2016 Central Italy earthquake sequence, *Earthquake Spectra*, EERI, 34(4), 1547-1555, doi:10.1193/080317EQS151M, 2018.

Tommasi, P., Di Giulio, A., Santo, A., Forte, G., De Falco, M., Verrucci, L., Lanzo, G., Rotonda, T., and Franke K.W.: Effects of the Central Italy 2016 seismic sequence on slope stability: Preliminary analysis of some major rock slides. *Proceedings,* 7th International Conference on Earthquake Geotechnical Engineering, ISSMGE, London, UK, 2019.

Tsou, C.Y., Chigira, M., Higaki, D., Sato, G., Yagi, H., Sato, H.P., Wakai, A., Dangol, V., Amatya, S.C., and Yatagai, A.: Topographic and geologic controls on landslides induced by the 2015 Gorkha earthquake and its aftershocks: an example from the Trishuli Valley, central Nepal. Landslides 15,953–965, https://doi.org/10.1007/s10346-017-0913-9, 2018

**FIGURES**

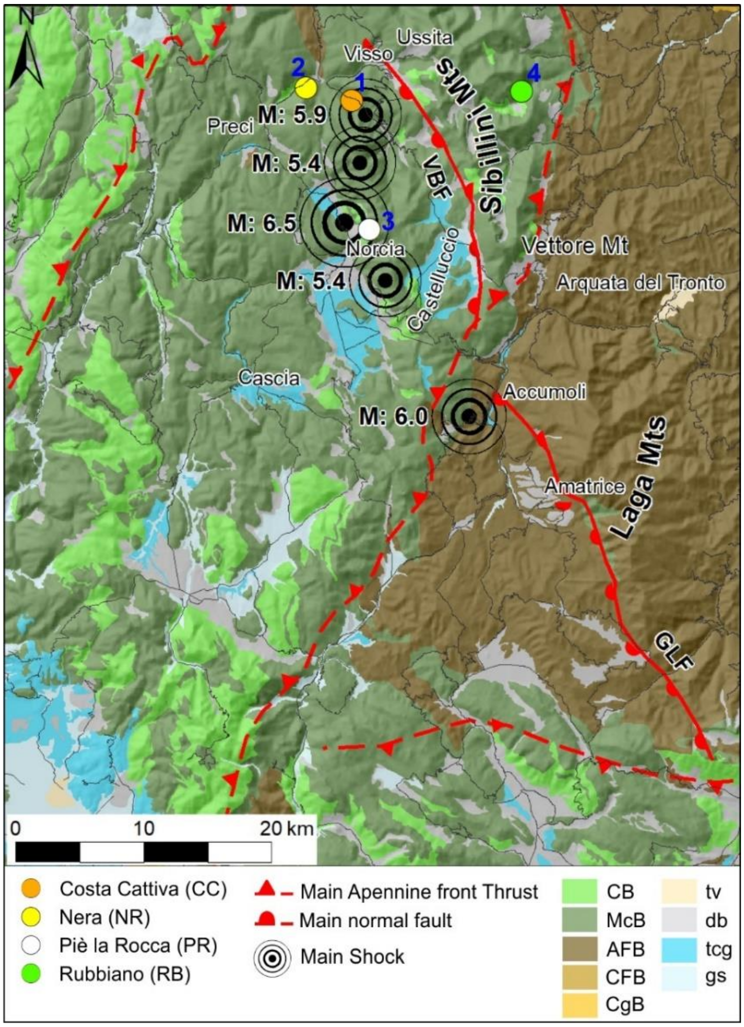


395 **Figure 1: Epicentres of the 2016–2017 CISS and location of the studied landslides on a simplified geological map (modified after Forte *et al.*, 2019). Keys: CB Carbonate Bedrock; McB Marly Carbonate Bedrock; AFB Arenaceous Flysch Bedrock; CFB Clayey Flysch Bedrock; CgB Conglomerate Bedrock; tv Travertine; db Debris; tcg terraced conglomerates; gs gravels and sands. GLF Gorzano – Laga Fault; VBF Vettore – Bove Fault.**

https://doi.org/10.5194/nhess-2022-256
Preprint. Discussion started: 24 October 2022




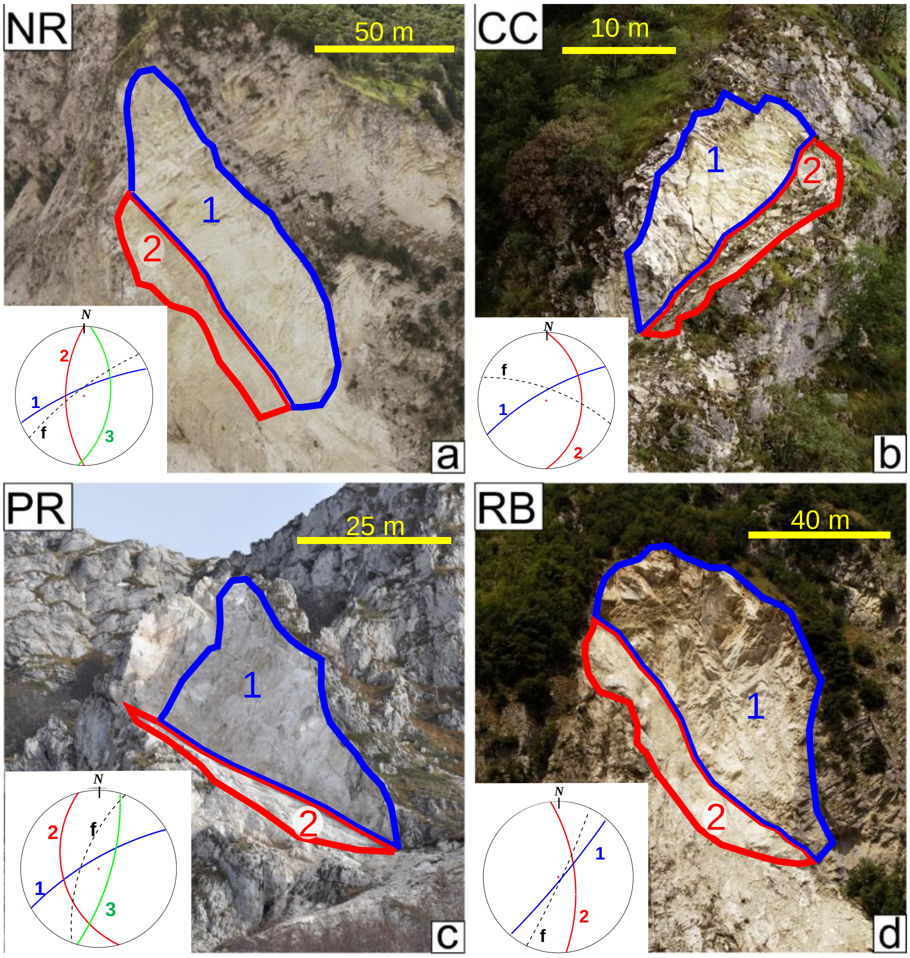


**Figure 2: Frontal view of the scars of the studied rockslides with approximated limits of the mean delimiting planes; a) Nera (NR); b) Costa Cattiva (CC); c) Piè la Rocca (PR); d) Rubbiano (RB). In the inner boxes: stereographic projections (lower hemisphere) of the discontinuity planes delimiting the failed masses (1, 2, 3) and of the local slope face (f).**

https://doi.org/10.5194/nhess-2022-256
Preprint. Discussion started: 24 October 2022


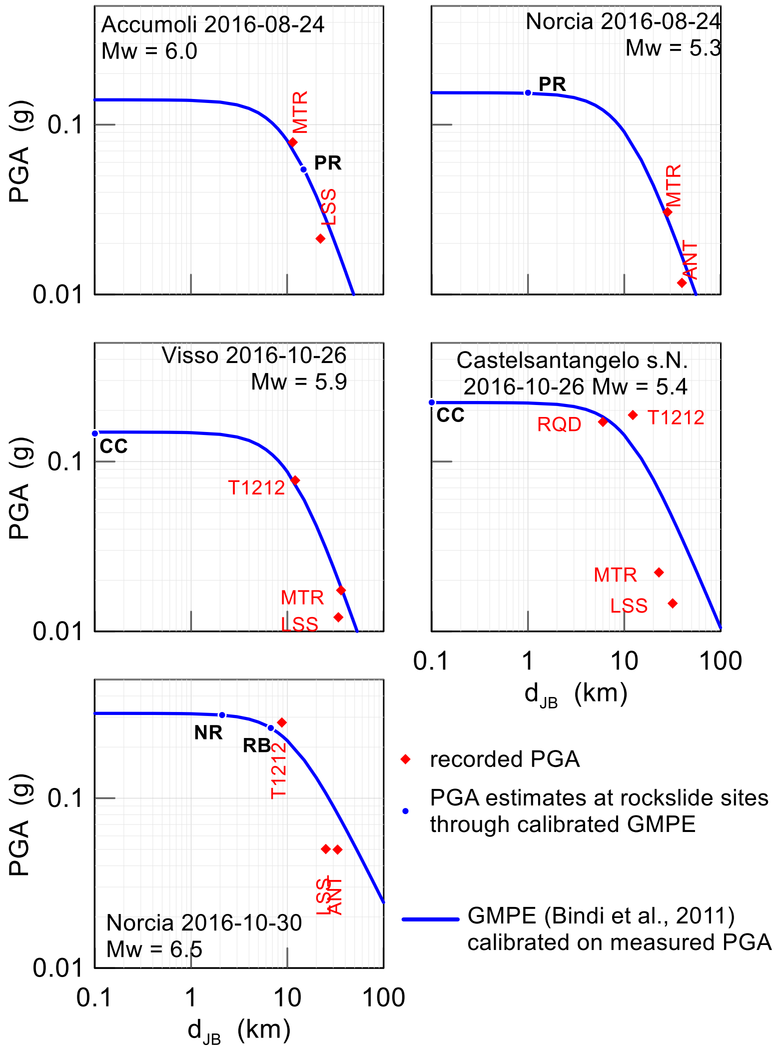


**Figure 3: PGA estimate through a calibrated GMPE for each shock. For PR rockslide and CC rockslide, two shocks are considered on August 24th and on October 26th respectively**

https://doi.org/10.5194/nhess-2022-256
Preprint. Discussion started: 24 October 2022

Natural Hazards and Earth System Sciences
Open Access
Discussions

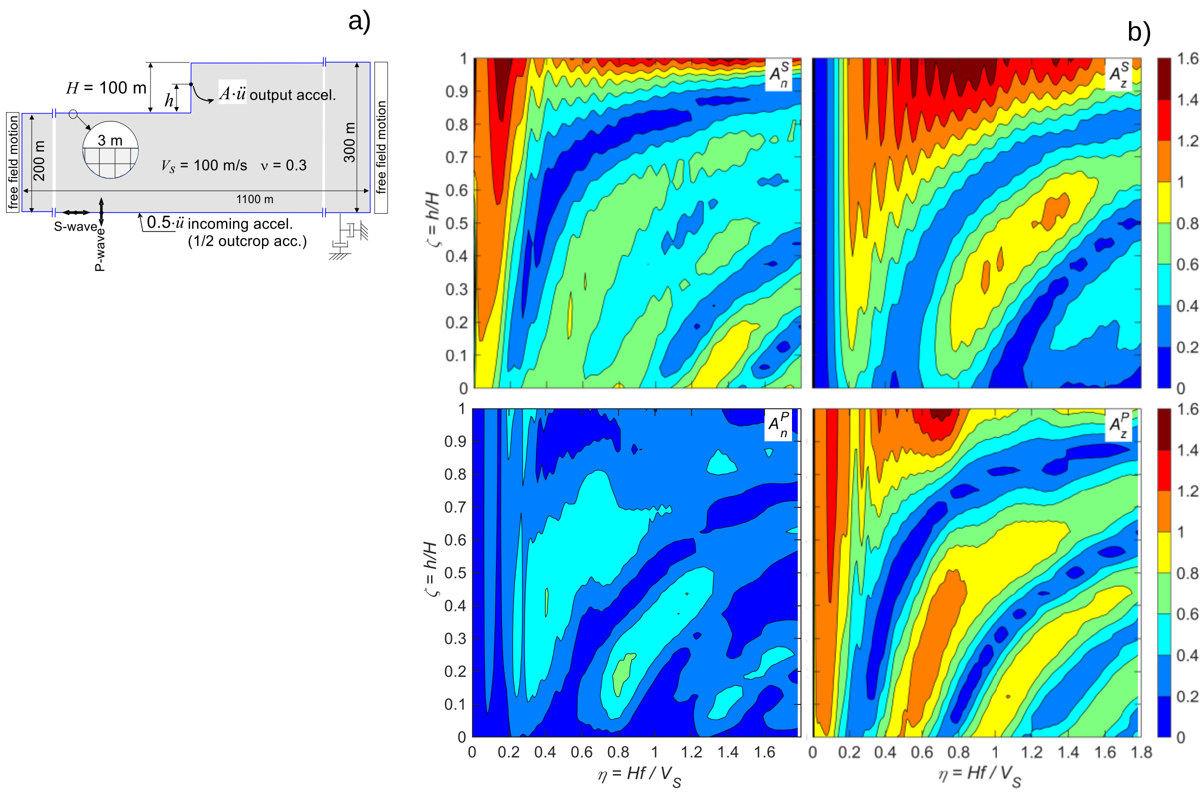


410

**Figure 4: Numerical model used for the seismic response of a vertical cliff (a). Amplification ratios with respect to the outcrop motion along the vertical wall of a step-like slope. Incident S wave ($A_n^S$ , $A_z^S$) and incident P wave ($A_n^P$ , $A_z^P$) (b).**

https://doi.org/10.5194/nhess-2022-256
Preprint. Discussion started: 24 October 2022




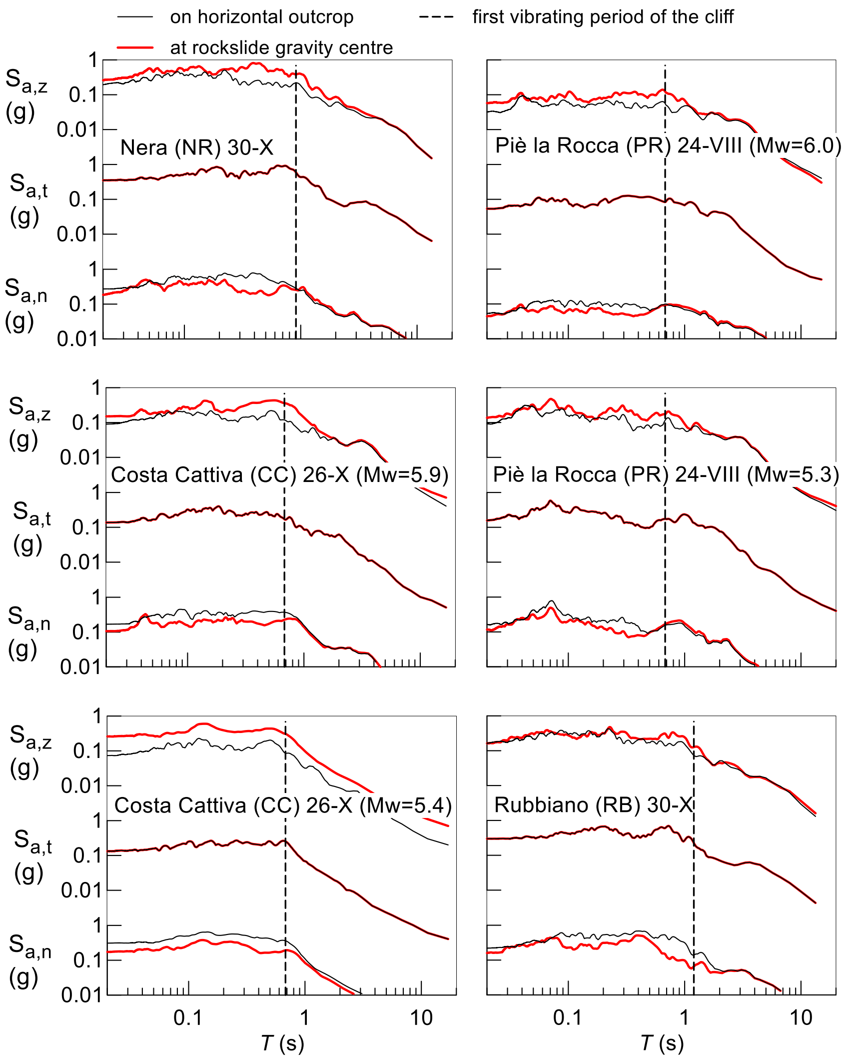


415 **Figure: 5: Response spectra of the three components of the acceleration at the rigid horizontal outcrop and on the vertical rock cliff at the elevation of the rockslide centre of mass as estimated through the seismic response of the numerical model for the four case studies (for each possible triggering earthquake).**

https://doi.org/10.5194/nhess-2022-256
Preprint. Discussion started: 24 October 2022


Natural Hazards and Earth System Sciences
Open Access
EGU
Discussions

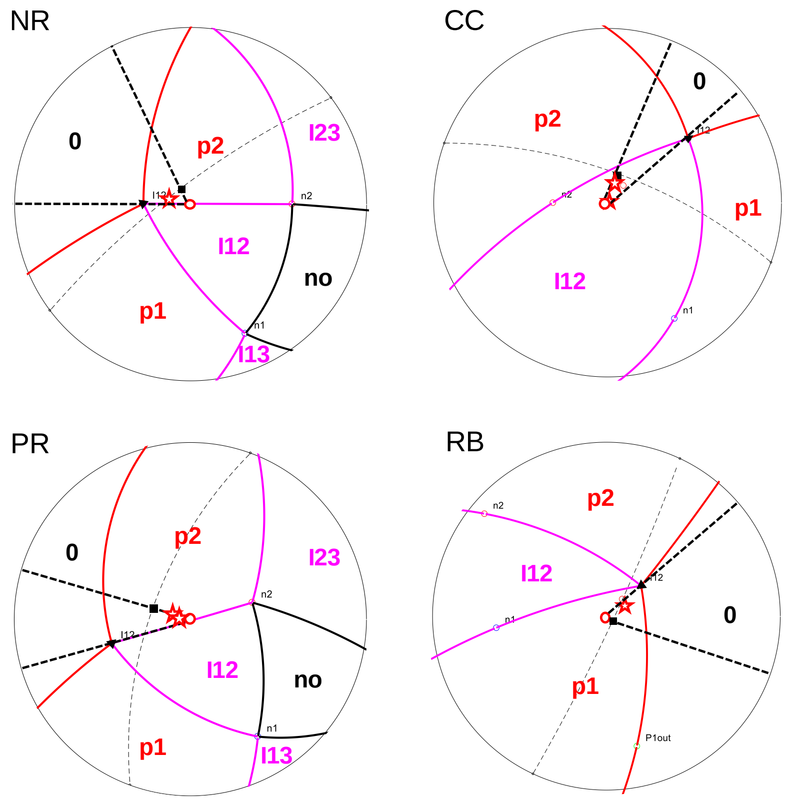


430 **Figure 6: Stereographic conform projections (lower hemisphere projected from upper focal point) of the trihedral/dihedral regions (solid lines) that define different sliding mechanisms depending on the direction of the resultant force. $I_{ij}$=sliding along the intersection line between the planes *i* and *j*, *pi*=sliding along the plane *i*. Light dashed lines are the projections of the average local slope face. Red stars indicate the resultant orientations corresponding to the minimum $F_s$ during the seismic shocks (see Fig. 8). Full triangles and squares indicate orientation of the intersection line ($I_{12}$) between the two planes and the dip direction of the slope face, respectively.**

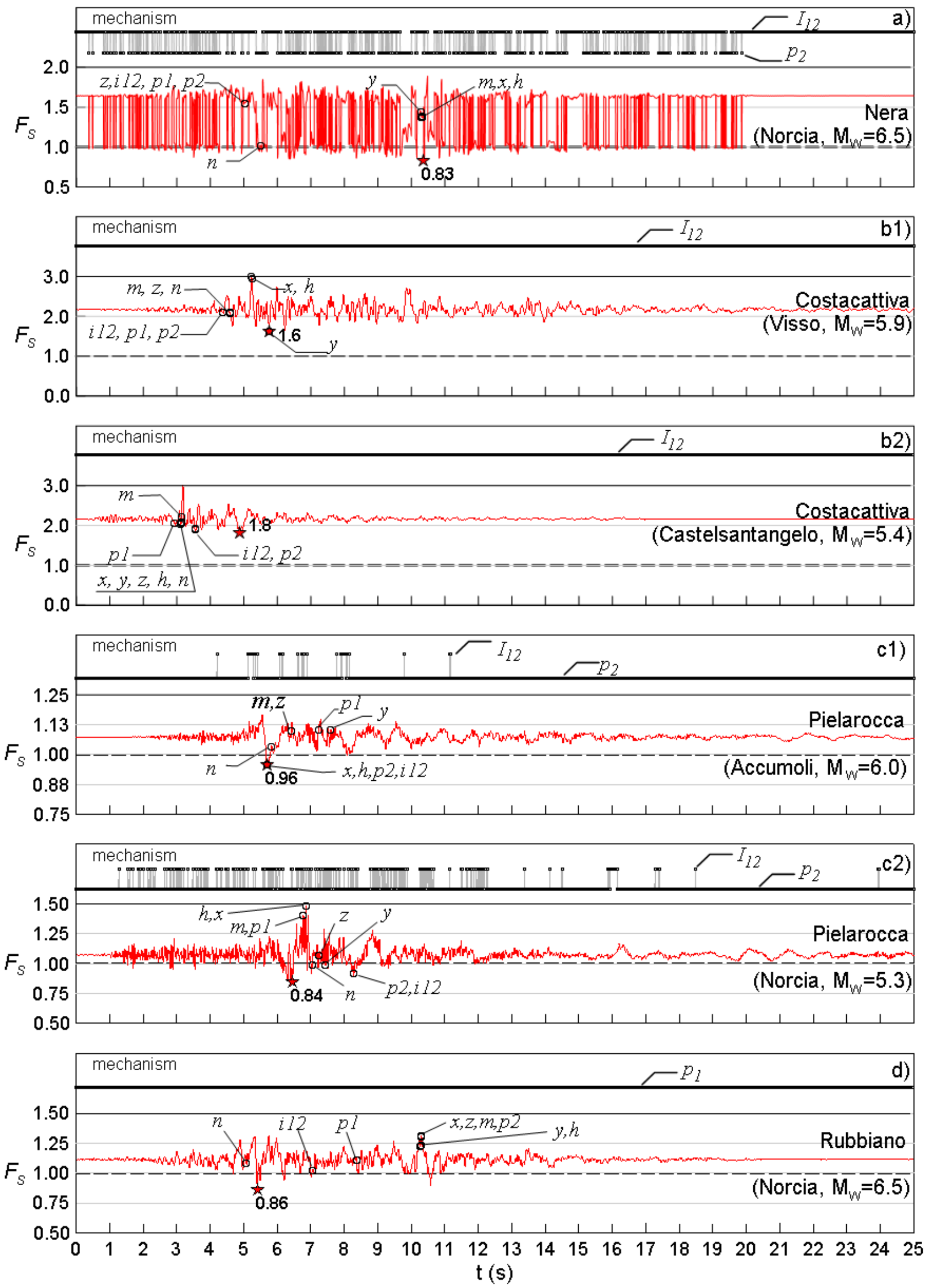


**Fig 7 Time histories of the safety factor $F_s$ during the triggering shocks and of the instantaneous active mechanism: $I_{12}$ = sliding along the intersection line between the planes, $p_1$, $p_2$ =sliding along the plane 1 and 2 respectively. Stars indicate minimum $F_s$. Empty circles highlight instants with peak values of specific acceleration components: *x,y* = geographic components (E,N), *z* = vertical component, *h* = horizontal component, *n* = component normal to the slope face, *i12* = intersection line of the sliding planes, *p1* and *p2* = dip directions of the sliding planes, *m* = instant of maximum acceleration magnitude.**

https://doi.org/10.5194/nhess-2022-256
Preprint. Discussion started: 24 October 2022

Natural Hazards and Earth System Sciences
Discussions

# TABLES

**Table 1: Main features of the investigated rockslides**

| Landslide | | Possible triggering Earthquakes (date, GMT, moment magnitude) | Estimated volume ($m^3$ x $10^3$) | Lithology |
|---|---|---|---|---|
| Nera (Sasso Pizzuto Mt.) | NR | October 30th 2016, 6:40:18, $M_W$=6.5 | 32.0 | *Layered limestones (Maiolica Fm.)* |
| Costa Cattiva (Nera River Valley) | CC | October 26h 2016, 17:10:36, $M_W$=5.4<br>October 26h 2016, 19:18:06, $M_W$=5.9 | 0.4 | » |
| Rubbiano (Infernaccio gorge) | RB | October 30th 2016, 6:40:18, $M_W$=6.5 | 15.0 | » |
| Piè la Rocca (Patino Mt.) | PR | August 24th 2016, 01:36:32, $M_W$=6.0<br>August 24th 2016, 02:33:29, $M_W$=5.3 | 15.0 | *Massive limestones (Calcare Massiccio Fm.)* |

**Table 2: Peak ground accelerations from the available records of the shocks at stations installed on rigid outcrop within 50 km from the epicentres of the seismic events.**

| Event | | | Seismic station | Epicentral distance | $D_{JB}$ | Horizontal E-W PGA | Horizontal N-S PGA | Vertical PGA |
|---|---|---|---|---|---|---|---|---|
| Epicentre | Date | $M_W$ | | km | km | $m/s^2$ | $m/s^2$ | $m/s^2$ |
| Accumoli | 2016-08-24 | 6.0 | IT.MTR<br>IT.LSS | 19.40<br>26.70 | 11.40<br>22.22 | 0.791<br>0.230 | 0.754<br>0.190 | 0.418<br>0.151 |
| Norcia | 2016-08-24 | 5.3 | IT.MTR<br>IT.ANT | 30.80<br>42.00 | 28.13<br>39.68 | 0.295<br>0.118 | 0.305<br>0.112 | 0.137<br>0.048 |
| Visso | 2016-10-26 | 5.9 | IV.T1212<br>IT.LSS<br>IT.MTR | 18.8<br>41.1<br>43.8 | 12.1<br>33.9<br>36.2 | 0.667<br>0.128<br>0.174 | 0.866<br>0.110<br>0.168 | 0.445<br>0.118<br>0.091 |
| Castelsantangelo sul Nera. | 2016-10-26 | 5.4 | IV.T1212<br>IV.RQT<br>IT.LSS<br>IT.MTR | 15.2<br>17.4<br>37.6<br>40.9 | 12.3<br>3.7<br>23.8<br>22.6 | 1.767<br>2.177<br>0.148<br>0.179 | 1.917<br>1.296<br>0.139<br>0.266 | 0.588<br>0.880<br>0.079<br>0.085 |
| Norcia | 2016-10-30 | 6.5 | IV.T1212<br>IT.LSS<br>IT.ANT | 10.50<br>32.60<br>46.10 | 8.77<br>25.10<br>33.27 | 2.744<br>0.464<br>0.436 | 2.731<br>0.523<br>0.546 | 1.636<br>0.399<br>0.242 |

**Table 3: Parameters of the triggering events utilized to calculate the motion at the rockslide sites from the available recorded accelerograms**

| Rockslide | | | | | | | | | |
|---|---|---|---|---|---|---|---|---|---|
| Site | lat. | long. | Seismic event | | | Epicentral distance | $D_{JB}$ | *S* | PGA * |
| | ° | ° | epicentre | date | $M_W$ | km | km | - | g |
| NR | 42.93 | 13.07 | Norcia | 2016-10-30 | 6.5 | 10.2 | 2.1 | 1.103 | 0.309 |
| RB | 42.93 | 13.28 | Norcia | 2016-10-30 | 6.5 | 16.8 | 6.7 | 0.926 | 0.259 |
| CC | 42.92 | 13.12 | Visso | 2016-10-26 | 5.9 | 2.3 | 0.0 | 1.862 | 0.146 |
| | | | Castelsant. | 2016-10-26 | 5.4 | 4.4 | 0.0 | 1.186 | 0.223 |
| PR | 42.82 | 13.13 | Accumoli | 2016-08-24 | 6.0 | 4.6 | 1.0 | 0.668 | 0.054 |
| | | | Norcia | 2016-08-24 | 5.3 | 16.3 | 14.8 | 1.890 | 0.154 |

* peak ground acceleration estimated at the site on rigid horizontal outcrop

https://doi.org/10.5194/nhess-2022-256
Preprint. Discussion started: 24 October 2022

Natural Hazards and Earth System Sciences Discussions
Open Access
EGU

**Table 4: Parameters utilized to calculate the topographic modification of the seismic motion at the rockslide sites**

| Rockslide | Dip direction of the slope face, $\alpha$ (°) | Cliff height, $H$ (m) | Height of the rockslide centre of mass, $h$ (m) | Period of first mode, $T_0$ (s) |
|---|---|---|---|---|
| Nera (NR) | 330 | 400 | 250 | 0.91 |
| Costa Cattiva (CC) | 330 | 300 | 90 | 0.68 |
| Rubbiano (RB) | 115 | 530 | 170 | 1.20 |
| Piè la Rocca (PR) | 330 | 300 | 180 | 0.68 |

**Table 5. Input parameters for the static LEM stability analyses after Forte *et al.* (2021)**

| rockslide | volume | plane 1 | | | plane 2 | | | plane 3 | LEM (static condition) | |
|---|---|---|---|---|---|---|---|---|---|---|
| | $m^3$ | dip/dd °/° | $\varphi_1$' ° | $A_{rb1}$ $m^2$ | dip/dd °/° | $\varphi_2$' ° | $A_{rb2}$ $m^2$ | dip/dd °/° | mechanism | $F_S$ - |
| NR | 30940 | 77/337 | 47 | 570+800 | 60/270 | 40 | 0 | 48/95 | line $I_{12}$ | 1.68* |
| CC | 400 | 75/330 | 47 | 0 | 35/090 | 40 | 0 | - | line $I_{12}$ | 2.16 |
| PR | 14000 | 75/330 | 47 | 0 | 40/255 | 42 | 0 | 72/106 | on plane 2 | 1.07 |
| RB | 15000 | 65/084 | 47 | 0 | 85/130 | 40 | 2880 | - | on plane 1 | 1.11** |

*: with the cohesive contribution of the spur at the lower wedge tip (800 $m^2$)
**: with the tensile contribution of the rear wedge surface (composite surface labelled as plane 2)
$A_{rb}$: areas of intact rock along the sliding planes providing cohesive contribution